crystals

MDPI

Article

A New L-Proline Amide Hydrolase with Potential Application within the Amidase Process

Sergio Martinez-Rodríguez [1,2,*], Rafael Contreras-Montoya [3], Jesús M. Torres [1], Luis Álvarez de Cienfuegos [3] and Jose Antonio Gavira [2,*]

[1] Department of Biochemistry and Molecular Biology III and Immunology, University of Granada, 18071 Granada, Granada, Spain; torrespi@ugr.es
[2] Laboratory of Crystallographic Studies, Andalusian Institute of Earth Sciences, C.S.I.C. University of Granada, Avenida de las Palmeras No. 4, 18100 Armilla, Granada, Spain
[3] Department of Organic Chemistry, University of Granada, 18071 Granada, Granada, Spain; rcm@ugr.es (R.C.-M.); lac@ugr.es (L.Á.d.C.)
* Correspondence: sergio@ugr.es (S.M.-R.); jgavira@iact.ugr-csic.es (J.A.G.)

Abstract: L-proline amide hydrolase (PAH, EC 3.5.1.101) is a barely described enzyme belonging to the peptidase S33 family, and is highly similar to prolyl aminopeptidases (PAP, EC. 3.4.11.5). Besides being an *S*-stereoselective character towards piperidine-based carboxamides, this enzyme also hydrolyses different L-amino acid amides, turning it into a potential biocatalyst within the Amidase Process. In this work, we report the characterization of L-proline amide hydrolase from *Pseudomonas syringae* (PsyPAH) together with the first X-ray structure for this class of L-amino acid amidases. Recombinant PsyPAH showed optimal conditions at pH 7.0 and 35 °C, with an apparent thermal melting temperature of 46 °C. The enzyme behaved as a monomer at the optimal pH. The L-enantioselective hydrolytic activity towards different canonical and non-canonical amino-acid amides was confirmed. Structural analysis suggests key residues in the enzymatic activity.

Keywords: amidase; amino acid; amidase process; proline; aminopeptidase; S33 family

Citation: Martinez-Rodríguez, S.; Contreras-Montoya, R.; Torres, J.M.; de Cienfuegos, L.Á.; Gavira, J.A. A New L-Proline Amide Hydrolase with Potential Application within the Amidase Process. *Crystals* **2022**, *12*, 18. https://doi.org/10.3390/cryst12010018

Academic Editors: Kyeong Kyu Kim and Dinadayalane Tandabany

Received: 25 November 2021
Accepted: 21 December 2021
Published: 23 December 2021

1. Introduction

L-proline amide hydrolase (PAH, EC 3.5.1.101) is a barely described enzyme, which up to now, has only been characterized with some detail in *Pseudomonas azotoformans* IAM 1603 (LaaA$_{Pa}$) [1,2]. PAH belongs to the serine peptidase S33 family, together with prolyl aminopeptidases (PAP, EC. 3.4.11.5) or prolinases (Pro-Xaa dipeptidase, 3.4.13.18). PAH was suggested as a different member of this family since LaaA$_{Pa}$ proved a different substrate scope than PAPs [2]. On the other hand, the enzyme proved enantioselective towards different piperidine-based carboxamides, L-prolinamide, and other different amino acid amides (Figure 1A). Since LaaA$_{Pa}$ was applied in the context of the so-called "Amidase Process" for the industrial production of optically pure amino acids, its different substrate scope prompted its nomenclature also as L-amino acid amidase [2–4]. This biotechnological process consists of the dynamic kinetic resolution of amino acid amides mixtures using an α-amino-ε-caprolactam racemase together with a stereoselective "D- or L-amidase" (Figure 1B, [3]).

As for other enzymes with biotechnological interest, the general "amidase" nomenclature might confuse neophyte and experienced researchers, since it includes different unrelated enzymes. The enzymatic resolution of the two isomers of proline amide (D and L) was already achieved using an "amidase" from hog kidney more than half a century ago [5]; this enzyme also proved useful for the resolution of diverse amino acid amides ([6] and references therein).

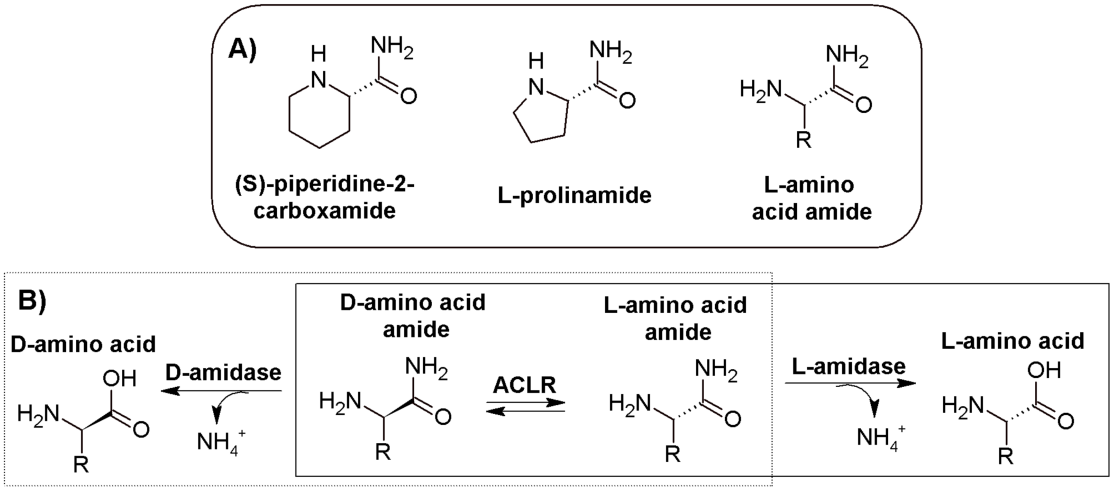

Figure 1. (**A**) Substrates recognized by L-proline amide hydrolase. (**B**) General scheme of the "Amidase Process". The full line represents the "L-system", whereas the dashed line represents the "D-system". ACLR: α-amino-ε-caprolactam racemase.

A reduced number of "L-amidases" have been studied to some detail, such as those from *Pseudomonas azotoformans* [1], *Ochrobactrum anthropi* [7,8], and *Brevundimonas diminuta* [2]. Enzymes from *Pseudomonas putida* [9] or *Mycobacterium neoaurum* ATCC 25795 [10], and different aminopeptidases (EC. 3.4.11.X) and amidases (E.C. 3.5.1.4) have also shown to able to hydrolyze amino acid amides with good enantioselectivity [11,12]. Some of the latter enzymes have been applied at the industrial level [9,11,12]. A discrete example of the hydrolysis of amino acid esters and amides by acylase I has been reported, despite this enzyme being mainly used for the hydrolysis of N-acetyl-amino acids [13]. Peptide amidase from *Citrus sinensis* and *Stenotrophomonas maltophilia* also allowed enzymatic resolution of racemic N-acetyl amino acid amides, yielding N-acetyl-L-amino acids with optical purity $\geq$ 99% [14]. As for the "amidase" nomenclature, PAPs present a similar scenario, whereas many of the reported PAPs show a clear preference for proline residues ([15] and references therein), not all cases show that they are obligate "proline aminopeptidases". Some members of this family have shown cleaving activity with different amino acid derivatives at different extents [15–17].

In order to gain understanding into enzymes with L-amidase activity and with potential industrial interest, we have embarked on the characterization of a putative PAP from *Pseudomonas syringae* (PsyPAH). This enzyme is highly similar to $LaaA_{Pa}$, which is the only PAH characterized showing L-amino acid amidase activity [1]. On the other hand, the closest structural homolog of PsyPAH to date is the amidohydrolase VinJ from *Streptomyces halstedii* (PDB 3WMR, 55% seq id.), with a highly different substrate scope [18]. In this work, we provide biochemical and biophysical characterization, together with the first X-ray structure of a PAH enzyme (PAP-like) with experimentally proven "L-amidase" activity. We have gone a step forward and based on sequence and structural information, we have categorized the different L-amidase enzymes in the literature in an attempt to facilitate comprehension on their potential biotechnological application.

2. Materials and Methods

The different amino acid amides and *p*-nitroanilide derivatives used for activity measurement of PsyPAH were purchased from VWR (VWR International Eurolab S.L, Barcelona, Spain), TCI chemicals, Alfa Aesar, or Acros (Cymit Quimica, Barcelona, Spain). Other amino acid amides were synthesized as previously described [19] (see supporting information). Other chemicals were from Sigma Aldrich (Sigma-Aldrich, St. Louis, MO, USA).

2.1. Cloning, Overexpression, and Purification of PsyPAH

A DNA sequence corresponding to the putative L-amidase from *Pseudomonas syringae pv. tomato* (Uniprot A0A0Q0CYJ4) was synthesized and cloned into pET-22b (NZYtech, Lisboa, Portugal) for over-expression in *Escherichia coli*. The resulting construct allows the overproduction of PsyPAH fused to a C-terminal His_6-tag. *E. coli* BL21 (DE3) (Agilent, Madrid, Spain) was transformed with this plasmid and grown in solid LB medium supplemented with 100 $\mu g \cdot mL^{-1}$ of ampicillin. A single colony was transferred into 10 mL of LB medium with ampicillin at the concentration above mentioned and incubated overnight at 37 °C. Then, 500 mL of LB supplemented with ampicillin was inoculated with 5 mL of the overnight culture. After 3–4 h of incubation at 37 °C with vigorous shaking, the OD^{600} of the resulting culture was 0.6–0.8. To induce the over-expression of PsyPAH, isopropyl-β-thio-D-galactopyranoside (IPTG) was added to a final concentration of 0.2 mM and the culture was kept at 16 °C overnight. Cells were collected by centrifugation (4000 rpm, 4 °C, 20 min) and subsequently frozen at −80 °C till use.

The pellet corresponding to 1 L was resuspended in 10 mL of 20 mM sodium phosphate, 20 mM of imidazole, and 300 mM of NaCl pH 8.0 (washing buffer, WB). Cells were lysed on ice via sonication with a Branson sonicator (6 periods of 60 s (1 s on, 1 s off), amplitude 25%) and then centrifuged (13,000 rpm, 10 min, RT). The resulting supernatant was applied to a HisPur Ni-NTA column (1 mL, Thermo Fisher, Waltham, MA, USA) previously equilibrated with 10 mL of WB. The column was then washed with 12 mL of WB and protein was eluted with 3 mL of 20 mM of sodium phosphate, 300 mM of imidazole, and 300 mM of NaCl pH 8.0. Subsequently, protein samples were loaded onto a Superdex 200 16/60 XK gel-filtration column (GE Healthcare, Boston, MA, USA) in an AKTA-prime FPLC system (GE Healthcare) using 20 mM of Hepes pH 7.0 as a running buffer. The peak corresponding to PsyPAH was concentrated up to 20 $mg \cdot mL^{-1}$ using 30 kDa concentrators (Amicon Ultra-Millipore) and dialyzed in 20 mM of Hepes pH 7.0 (4 °C). Protein was frozen at −80 °C till use. Protein purity was verified by SDS-PAGE. Protein concentrations were determined from the absorbance at 280 nm (ε = 49,390 $M^{-1} \cdot cm^{-1}$).

2.2. Activity Measurement

Different amino acid amides (10 mM) were used as possible substrates for PsyPAH: (amide derivatives of Gly, L-Pro and D-Pro, L-Trp, L-Phe, L-*tert*-Leu, L-Ala, L-norVal, L-Met, L-homoPhe, L-Ser, L-norLeu, L-Leu, L-2-ABA, and L-Val). The phenate method was used to measure ammonia formation [20], with slight modifications. Reaction volumes of 200 µL and a final enzyme concentration of 0.1–0.2 $mg \cdot mL^{-1}$ (pH 7.0, 35 °C) were used. After 5–15 min, the reaction was stopped by mixing with 540 µL of freshly prepared phenate solution. A total of 280 µL of 2.5% sodium hypochlorite and 140 µL of 25 µM $MnCl_2$ were then added, followed by incubation at 70 °C for 40 min. Absorbance was measured at 625 nm. $(NH_4)_2SO_4$ standards were used for all the assays. Three replicates were conducted for each experiment.

Kinetic parameters for L-prolinamide and L-leucinamide were calculated with substrate concentrations ranging 0.1 to 15 mM, using 100 mM of stock solutions (in 100 mM of phosphate buffer pH 7.0). Reactions were carried out at 35 °C and pH 7.0 (using 20–400 $\mu g \cdot mL^{-1}$ PsyPAH concentrations depending on the substrate). After 5–15 min, (pre-experiments suggested this reaction time as appropriate for Vo calculation), ammonium formation was measured with the phenate method (see above). The activity with *p*-nitroanilide derivatives was measured following sample absorption at 405 nm. K_m and k_{cat} were measured using L-Leu and L-Pro *p*-nitroanilide concentrations ranging from 0.1 to 10 mM, using 500 mM of stock solutions (in acetonitrile). Reactions were carried out at 35 °C and pH 7.0 (using 8–80 $ng \cdot mL^{-1}$ PsyPAH concentrations depending on the substrate, with a constant 2% concentration of acetonitrile into the reaction). A calibration was performed and plotted with *p*-nitroaniline in the same buffer used for activity determination (experimental ε = 9265 $cm^{-1} \cdot M^{-1}$, similar to that reported previously [21]). Three replicates were conducted for each experiment.

2.3. Size Exclusion Chromatography (SEC-FPLC)

PsyPAH was loaded onto a Tricorn Superdex 200 gel-filtration column (GE Healthcare) using an AKTA-prime FPLC system (GE Healthcare), with 20 mM of sodium phosphate pH 7.0 as a running buffer. BSA (66 kDa), ovalbumin (43 kDa), carbonic anhydrase (29 kDa), and RNase A (13.7 kDa) were used as standards for molecular mass determination (Cytiva Gel Filtration Calibration Kits).

2.4. Dynamic Light Scattering

DLS measurements were performed in a Zetasizer Nano instrument (Malvern Instruments Ltd., Malvern, UK). Experiments were performed with PsyPAH (1.3 mg·mL^{-1}) in 20 mM of sodium phosphate pH 7.0 at 25 °C. Samples were centrifuged for 10 min at 13,000 rpm before measurement. The PsyPAH sample was measured 3 times with 10 runs each (in automatic mode for time selection).

2.5. Thermal Shift Assays

Thermal shift assays were carried out using a QuantStudio 3 qPCR (Thermo Fisher). A concentrated PsyPAH sample was 10-fold diluted directly into different 100-mM buffers (sodium acetate, pHs 4.0–5.6; sodium phosphate, pHs 6.0–8.0; tetraborate HCl/NaOH, pHs 8.0–10.0) to a final concentration of 1.4 mg·mL^{-1}, and kept at 4 °C O/N. Aqueous SYPRO (50×) was added to a final 10× concentration. Thermal denaturation measurements were monitored by measuring the changes in the fluorescence as a result of SYPRO binding. Denaturation data were collected from 25 to 99 °C at a scan rate of 3 °C·min^{-1}. Three replicates were conducted in all cases. Despite the irreversibility of the thermal unfolding, apparent Tms were calculated using a Boltzmann fit to the raw data, with Protein Thermal shift software v1.3 (Thermo Fisher).

2.6. Crystallization

Freshly purified recombinant His_6-tagged PsyPAH (20 mg·mL^{-1}, 20 mM of Hepes pH 7.0) was used to set up initial crystallization screenings with the HRCS I & II (Hampton Research, Palo Alto, CA, USA). The hanging drop configuration of the vapor diffusion method with a 1:1 ratio of the reservoir and protein solution was used. Crystallization experiments were kept at 20 °C in an incubator. Crystals were obtained using 0.2 M of sodium acetate trihydrate, 0.1 M of sodium cacodylate trihydrate pH 6.5, and 30% w/v polyethylene glycol 8000 after 48 h.

2.7. Data Collection and Refinement

Target crystals were identified under a microscope using polarized light, separated with a microtool, fished out of the drop with a loop, and transferred to a 1-µL drop of mother solution containing 20% (v/v) glycerol as cryo-protectant. After soaking for less than 60 s, crystals were flash-cooled in liquid nitrogen and stored until data collection.

X-ray diffraction data were collected at ID30B (ESRF, Grenoble, France). Diffraction data were indexed and integrated using XDS [22] and scaled with AIMLESS from the CCP4 suite [23]. The crystal structure of PsyPAH was determined by the molecular replacement method with PHASER [24] using the structure of the amidohydrolase VinJ from *Streptomyces halstedii* (PDB ID: 3WMR) [18] as the search model. Refinement was done with PHENIX [25] and Refmac [26] with cycles of manual rebuilding using COOT [27] and finalized using several cycles of refinement applying TLS parameterization [28]. The final refined model was checked with Molprobity [29]. Data collection and refinement statistics are summarized in Table 1.

Table 1. Data collection and refinement statistics. (Statistics for the highest-resolution shell are shown in parentheses.)

Data Collection	
Source	ESRF ID30B
Space group	P 21 21 21
Cell dimensions	
a, *b*, *c* (Å)	49.428, 65.033, 85.016
α, β, γ (°)	90.0, 90.0, 90.0
Resolution (Å)	42.73–1.95 (2.02–1.95)
Unique reflections	20,565 (2016)
$I/\sigma I$	7.2 (1.8)
Completeness (%)	99.70 (99.75)
Redundancy	5.1 (5.1)
R_{merge}	15.7 (91.9)
$CC_{1/2}$	0.991 (0.636)
Refinement	
R_{work}/R_{free}	15.68/22.25
No. atoms	2824
Protein	2571
Ligand/ion	5
Water	248
B-factors	21.97
Protein	20.95
Ligand/ion	30.16
Water	32.35
R.m.s. deviations	
Bond lengths (Å)	0.007
Bond angles (°)	0.85
PDB ID	7A6G

2.8. Sequence and Structure Analysis

PDB-SUM was used for global structure analysis [30]. Clustal omega [31] and SPript [32] were used for multiple sequence alignment and phylogenetic analysis. The i-Tol server was used for tree representation [33]. The Dali server [34] was used to search for other members of the peptidase S33 superfamily with a similar fold to that presented by the PsyPAH structure. Graphical representation of 3D structural models was conducted with Pymol [35].

3. Results and Discussion

3.1. PsyPAH Characterization

Recombinant C-His_6-tagged PsyPAH was purified using nickel affinity chromatography and SEC-FPLC (Size-exclusion chromatography-Fast Protein Liquid Chromatography) (>95% purity, yield of 10 mg per L of culture). SEC-FPLC showed an estimated molecular mass of 33 ± 2 kDa in phosphate buffer pH 7.0 (Figure 2A), slightly lower than the theoretical molecular mass of the monomer (36.7 kDa). An estimated R_h of 2.5 ± 0.40 nm was obtained for PsyPAH by DLS (20 mM phosphate pH 7.0). This value is a bit higher than that shown for carbonic anhydrase (29 kDa, 2.37 nm [36]), and argues with the value obtained by SEC-FPLC. Thermal Shift Assays (TSA) showed single thermal transitions in the pH range from 6.0 to 11.0 as a result of SYPRO binding (Figure 2B, inset).

Apparent thermal midpoints (T_m^{app}) could be calculated from Boltzmann fitting, with values ranging from 35.8 to 46.0 °C in that pH interval (Figure 2B). The maximum T_m^{app} value coincided with the optimum pH activity of the enzyme (pH 7.0; Figure 2C). The optimal reaction temperature was 35 °C (Figure 2D), whereas enzymatic activity was lost at 50 °C.

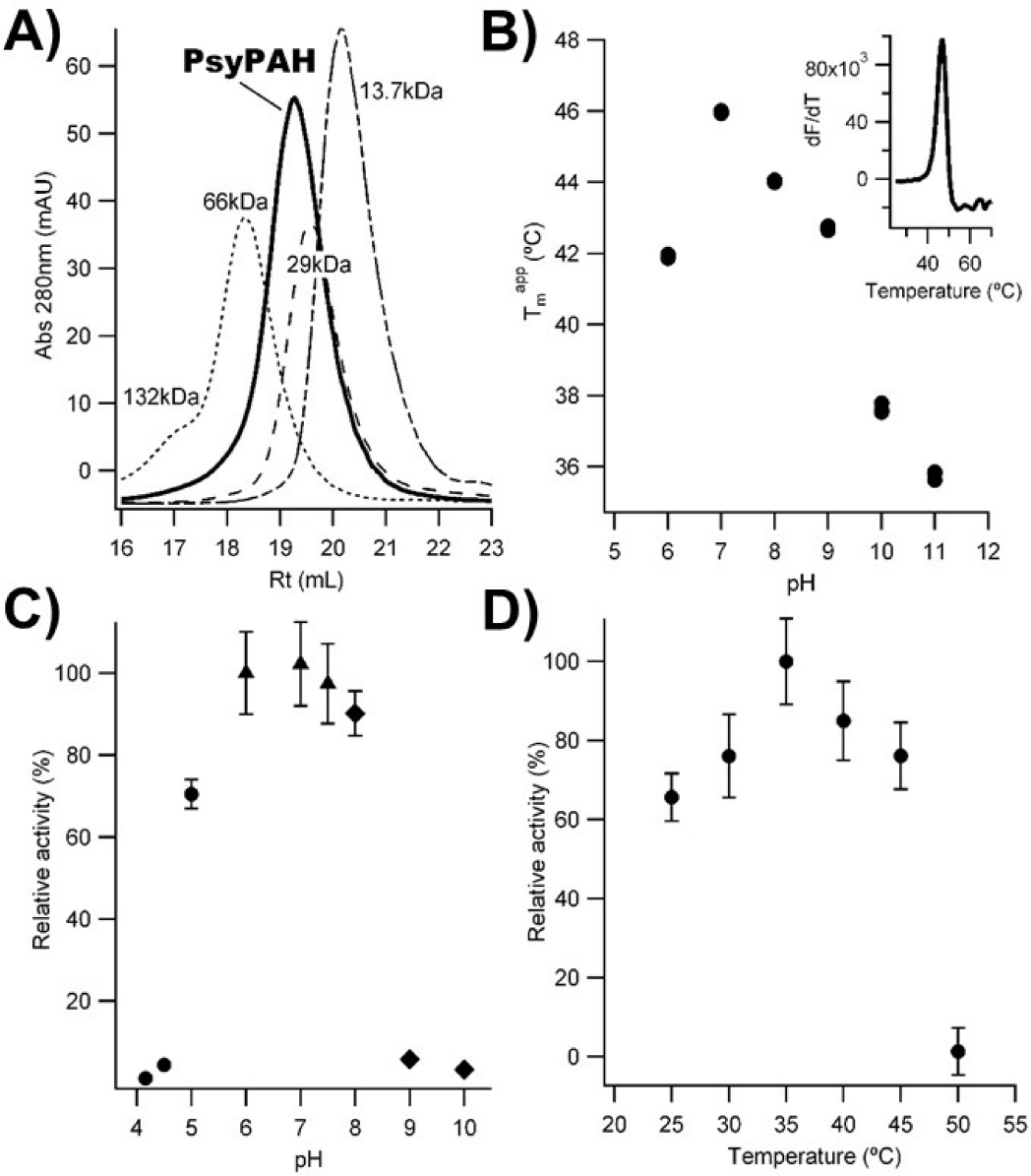

Figure 2. (**A**) SEC-FPLC of PsyPAH (black continuous line) in phosphate buffer 20 mM pH 7.0. Protein standards represented in dashed lines are BSA (132 and 66 kDa), carbonic anhydrase (29 kDa), and RNAse A (13.7 kDa). (**B**) Apparent T_ms calculated for PsyPAH at different pHs. The inset corresponds to the TSA experiment of PsyPAH in phosphate buffer at pH 7.0. Relative activity of PsyPAH as a function of pH (**C**) and Temperature (**D**).

Both the optimal temperature and pH were lower than those reported previously for $LaaA_{Pa}$ [2]. No activity loss was observed after incubation of PsyPAH at 30 °C for 14 h and it also retained over 75% of its activity after incubation at 35 °C for the same period of time. PsyPAH stored at −80 °C maintained full activity for more than two years. Biochemical parameters of PsyPAH were assayed with the amide and *p*-nitroanilide derivatives of L-Pro and L-Leu (Table 2), showing the expected L-amidase activity of the enzyme. Whilst, we could not determine the K_m values for two of the substrates used due to the limit of detection of the method (L-Pro-*p*-nitroanilide) and the solubility of the substrate (L-Leu-amide), visual inspection of the kinetic profiles (Figure S1) supports that the K_m for the amide derivatives of L-Pro and L-Leu is, at least, one order of magnitude higher than for the *p*-nitroanilide derivative (Table 2 and Figure S1). These results suggest that the presence

of the aromatic aniline moiety of the substrate improves PsyPAH-binding, which might reflect a better accommodation of these substrates into the active site.

Table 2. Kinetic parameters of PsyPAH with L-Pro and L-Leu amide and *p*-nitroanilide derivatives (pH 7.0, 35 °C). * Could not be determined due to detection limit of the determination method. ** Could not be determined due to the solubility of this substrate. *** Obtained from the linear part of the kinetic plot (see Figure S1).

Substrate	K_m (mM)	k_{cat} (s^{-1})	k_{cat}/K_m ($s^{-1} \cdot mM^{-1}$)
pN-Pro	ND *	445.38 ± 19.17	ND *
pN-Leu	1.14 ± 0.21	71.25 ± 3.34	62.5 ± 3.37
L-Pro amide	9.48 ± 1.6	14.03 ± 1.26	1.48 ± 0.13
L-Leu amide	ND **	ND **	0.03 ± 0.00 ***

We have also qualitatively tested the activity of PsyPAH towards different canonical and non-canonical L-amino acid amides. PsyPAH was able to hydrolyze glycinamide, L-alaninamide, L-phenyalalaninamide, L-methioninamide, L-serinamide, L-valinamide, L-tryptophanamide, L-norvalinamide, L-homophenylalaninamide, L-norleucinamide, and L-2-aminobutyramide (data not shown). No activity was detected towards D-prolinamide or L-tert-leucinamide.

3.2. PsyPAH Sequence Analysis

Since E.C. classification is based solely on the enzymatic reaction, different enzymes catalyzing the same reaction can share the same nomenclature (e.g., L-amidases), even when their sequences are highly different. This is a recurrent issue in the biotechnological field, where it is common to discover novel enzymes after screening methods for a desired specific activity, from which they are named. The general "amidase" nomenclature used in the context of the "Amidase Process" might thus initially confuse neophyte researchers in this field, since many different enzymes classified under E.C. 3.5.1 are named as "amidases" [12,37]. Previous studies on L-amidases of biotechnological interest already highlighted enzymes belonging to different protein families [2,12].

Phylogenetic analysis of the primary sequence of enzymes with L-amidase activity shows four different enzyme groups (Table 3 and Figure S2). The broad-spectrum amidase from *Ochrobactrum anthropi* [7] shapes an alternative "acetamidase/formamidase clan" (Pfam PF03069), together with the enzymes from *Enterobacter cloacae* and *Thermus* sp. (Table 2). The industrially-used L-amidase from *Pseudomonas putida* (a leucine aminopeptidase [9]) and $LaaA_{Bd}$ shape an alternative "aminopeptidase clan", belonging to the peptidase M17 family (Pfam PF00883). On the other hand, the leucyl-aminopeptidase from *Aeromonas proteolytica* [38] confers an isolated clan, which belongs to the peptidase M28 family (Pfam PF04389, Table 3). Finally, $LaaA_{Pa}$ and PsyPAH are grouped into a "peptidase S33 clan".

Thus, from a biotechnological point of view, it is important to bear in mind that different "L-amidases" belonging to different protein families exist when dealing with the so-called "Amidase Process". Besides their application on the production of amino acids, some of these L-amidases have also found other biotechnological applications [37,39,40], further increasing their potential and economic interest.

Table 3. Different enzymes with L-enantioselective amidase activity described in the literature with potential application in the production of amino acids. * It is not clear from the literature whether the hog kidney amidase used in the 50s for the resolution of amino acids [5,6] might correspond to a leucyl aminopeptidase or a PAP, or even if they are the same enzyme [41,42].

Acronym	Protein Family	Source	Sequence	Reference
PsyPAH	Serine peptidase S33	*Pseudomonas psyringae*	A0A0Q0CYJ4	This work
$LaaA_{Pa}$	Serine peptidase S33	*Pseudomonas azotoformans*	BAD15092.1	[1]
$LaaA_{Oa}$	Acetamidase/formamidase	*Ochrobactrum anthropi*	AAV87210	[7]
$LaaA_{Ec}$	Acetamidase/formamidase	*Enterobacter cloacae*	AAR56843	[43]
$LaaA_{Ts}$	Acetamidase/formamidase	*Thermus* sp.	BAL49703.1	[44]
XfAmid	Acetamidase/formamidase	*Xantobacter flavus*	BAE02548.1	[45,46]
$LaaA_{Bd}$	Leucine aminopeptidase (M17)	*Brevundimonas Diminuta*	BAE91931	[2]
ppLAP	Leucine aminopeptidase (M17)	*Pseudomonas putida*	CAA09054.1	[9]
apLAP	Leucyl-aminopeptidase (M28)	*Aeromonas proteolytica*	Q01693	[38]
$LaaA_{Mn}$	-	*Mycobacterium neoaurum*	n.a.	[10]
-	- *	*Hog kidney*	- *	[5]

3.3. Overall Structure of PsyPAH

PsyPAH crystallized in the most standard space group P212121 and presents a single polypeptide chain in the asymmetric unit, as observed in the solution. As ascertained from primary sequence analysis, PsyPAH belongs to the hugely diverse α/β hydrolase superfamily and more specifically to the serine peptidase family S33 (clan SC) [47]. The α/β hydrolase fold family of enzymes is one of the largest groups of structurally related enzymes with diverse catalytic functions. It contains several enzymes found to have a second promiscuous function on alternative substrates [48,49]. Like other members of this family, PsyPAH is constituted by two different domains, namely the catalytic domain (residues 1–141 and 231–end) and the cap domain (residues 142–230; Figure 3). The catalytic domain is formed by a αβα sandwich containing the conserved catalytic triad motif of the family (Ser113, Asp253, His280), whereas the cap domain is constituted exclusively by α-helices. A DALI search shows more than 140 structures with a Z-score over 20 when using the PDB90 subset database. However, only three structures present a sequence similarity over 25% with PsyPAH (Table S1): The amidohydrolase VinJ from *Streptomyces halstedii* (PDB 3WMR, 55% seq id. [18]), a putative uncharacterized PAP from *Mycobacterium smegmatis* (MysPAP, PDB 3NWO, 50% seq id.), and the Tricorn protease-interacting aminopeptidase F1 from *Thermoplasma acidophilum* (APF1, 34% seq. id., PDB 1MU0, [50], with RMSD of 1.0, 2.2, and 1.7 Å, respectively). Other different peptidase S33 family members appear with sequences below 21%, such as epoxide hydrolases and esterases (Table S1). On the other hand, other characterized PAPs included in the ESTHER database [51] whose structures are known, present a lower structure similarity with PsyPAH. This is the case of *Xanthomonas campestris* PAP (XcPAP, PDB 1AZW, [52]) or *Serratia marcescens* PAP (SmPAP, PDB 1QTR, [53]). Other known PAP family structures are those from the PAP-related protein TTHA1809 from *Thermus thermophilus* (PDB 2YYS, [54]) and putative PAP from yeast *Glaciozyma antarctica* (PDB 5YHP, unpublished results). However, no biochemical data is available for these enzymes.

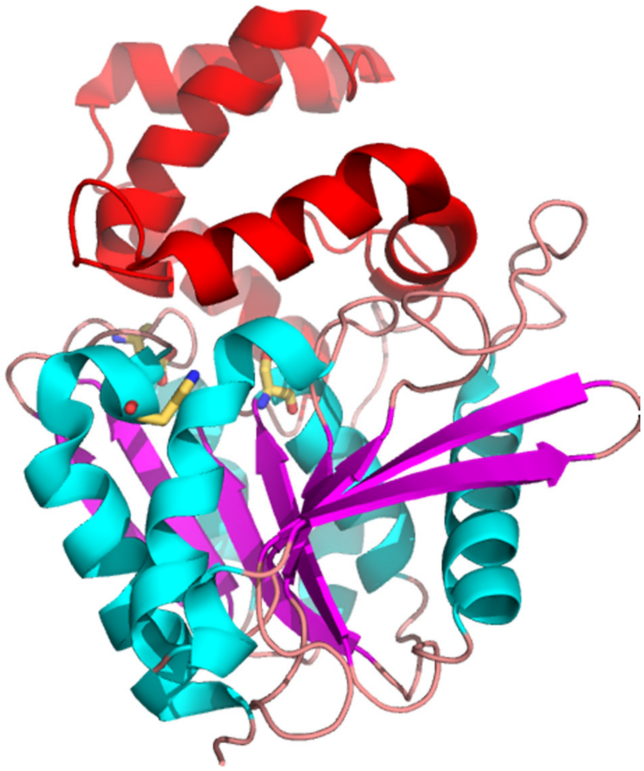

Figure 3. Overall fold of PsyPAH. The catalytic domain is shown in cyan/purple, whereas the cap domain appears in red. The catalytic triad (Ser113, Asp253, His280) is shown in stick mode to account for its position in the catalytic domain.

3.4. Differences on the Substrate Binding Groove (SBG) Seem to Account for the Substrate Scope of PsyPAH

The substrate specificity and function of prolyl peptidases was proposed early on to be determined by the cap domain [53], where the substrate firstly needs to bind before reaching the catalytic center to be hydrolyzed. The specificity of the exopeptidase activity of SmPAP was thus proposed to have originated by steric impediments of this smaller domain, which would block the entrance of extra residues at the N-terminal proline of the substrate [53]. Differences on the substrate binding entrance were already highlighted for APF1, XcPAP, and SmPAP, with the latter showing larger openings to the active site [50]. An overview of the homolog PsyPAH structures reveals that whereas the catalytic domains are spatially conserved, the cap domain presents clear positional differences (Figure 4). Interestingly, the highest differences in the cap domain are observed when comparing PsyPAH with the two characterized PAPs: XcPAP and SmPAP (Figure 4A), while better fit are observed with VinJ, APF1, and the uncharacterized MysPAP (Figure 4B). The substrate binding groove of APF1 (SBG, also known as E1 site [50,55]) was experimentally deciphered between two helices comprised in the cap domain (e.g., PDB 1XRP, Figure 5A); conservation of the spatial disposition of the SBGs into the cap domains of PsyPAH, VinJ, and MysPAP is observed (Figures 5 and S3), revealing clear differences on the different PAP structures: The SBG on XcPAP (and SmPAP) is in a completely different position to the other enzymes, in-between the cap and the catalytic domains (Figure 4A, [53]). The different position of the SBG makes the catalytic center more accessible to the solvent in XcPAP and SmPAP, supporting the acceptance of long peptides. However, in APF1, the N-terminal peptide needs to enter the catalytic center by a narrow hollow, where it can be processed [50,55]. This "smaller" SBG supports the acceptance of shorter peptides when compared with XcPAP and SmPAP. This should also be the case for PsyPAH as observed by the SBG configuration (Figures 4, 5 and S3).

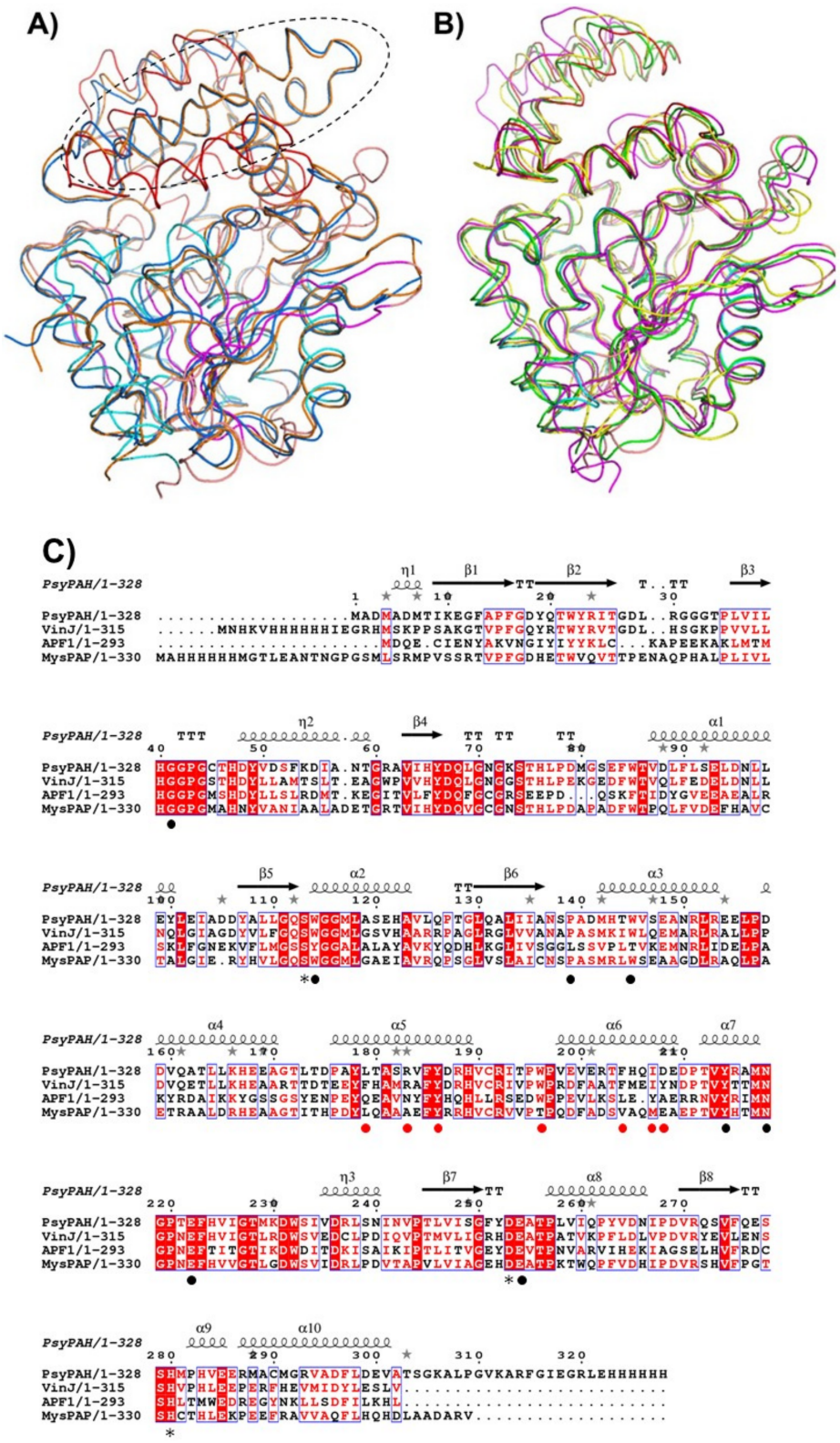

Figure 4. (**A**) Superposition of PsyPAH with "real" PAPs belonging to *Xanthomonas campestris* (XcPAP, PDB 1AZW) and from *Serratia marcescens* (SmPAP, PDB 1QTR). (**B**) Superposition of PsyPAH, amidohydrolase VinJ (PDB 3WMR), APF1 from *Thermoplasma acidophilum* (PDB 1MTZ), and putative uncharacterized PAP from *Mycobacterium smegmatis* (MysPAP, PDB 3NWO). (**C**) Sequence alignment of PsyPAH, VinJ, APF1, and MysPAP shown in panel B. Residues comprising the SBGs (red circles) or catalytic triad (asterisks)/catalytic cleft (black circles) are highlighted.

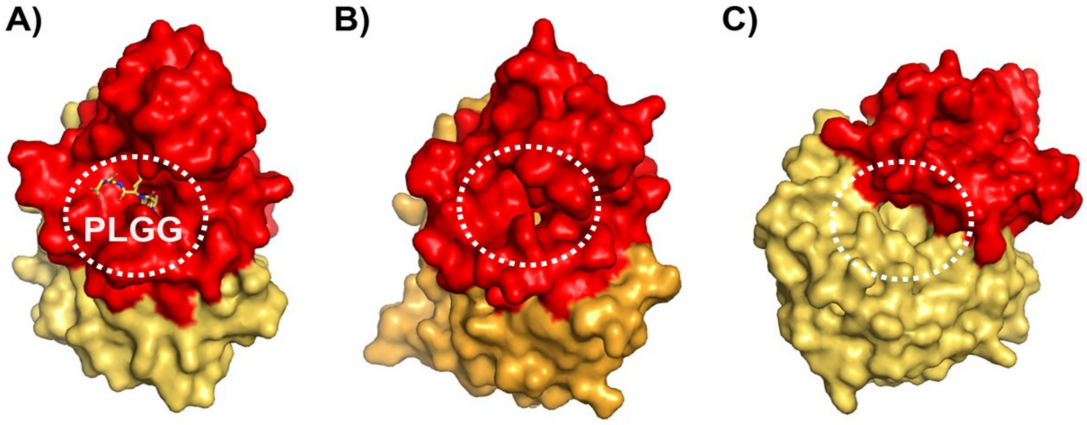

Figure 5. (**A**) Surface representation of APF1 showing the binding site of the tetrapeptide PLGG (E213Q mutant, PDB 1XRP). Red: Cap domain; orange: Catalytic domain. (**B**) Surface representation of PsyPAH showing the putative substrate binding site. Red: Cap domain; orange: Catalytic domain. The orientation is exactly the same as in (**A**). (**C**) Surface representation of XcPAP showing the putative substrate binding site. Red: Cap domain; orange: Catalytic domain. The orientation has been rotated approximately 90° with respect to (**A**).

The closest structural homolog of PsyPAH known to date is VinJ [18], but the most and only exhaustive analysis of the binding mode among homolog structures has been carried out with APF1 [50] (Table S2). Comparison of residues comprising different regions of APF1 (E1, S1, S1′ [50,55]) with those of PsyPAH, VinJ, and MysPAP reveals totally conserved residues, despite a low overall conservation (Table S3). The different substrate scope of VinJ compared to APF1 was explained by the presence of a unique polyketide binding tunnel (which partly correspond to the E1 site, Tables S3 and S4) and a smaller S1 site in VinJ [18]. These unique feature of VinJ is necessary for polyketide moiety fitting on the surface of the enzyme (and other VinJ-proteins used for the synthesis of β-amino acid containing macrolactams [18]). Comparison of this hydrophobic tunnel with PsyPAH, APF1, and MysPAP confirms the unique character of this binding site in VinJ, which shows an overall higher hydrophobic character (Figure S4, Table S4). Specifically, residues $F176^{VinJ}$ and $Y205^{VinJ}$ were hypothesized to provide additional hydrophobic interactions with the polyketide chain of the substrate [18]. However, counterpart residues in PsyPAH, APF1, and MysPAP are overall more polar (Table S4). In this sense, $E200^{APF1}$ (counter part of $Y205^{VinJ}$) has been experimentally proven to be responsible for peptide docking [55], (see below). These structural differences suggest that PsyPAH is not a VinJ-type protein, and also supports a closer binding mode and catalytic mechanism to that reported for APF1 (Table S4).

Different Proline-containing liganded structures of APF1 (Table S2), PDBs 1XQY, 1XRP, and 1XRR, [55] show $Y178^{APF1}$ and $E200^{APF1}$ as responsible for Pro-docking at the E1 site (Figure 6). The counterpart of $Y186^{PsyPAH}$ and $D208^{PsyPAH}$ residues plausibly have a key role in substrate positioning at PsyPAH; in fact, $D208^{PsyPAH}$ shows alternative orientations, suggesting a dynamic character for substrate binding. A lower volume of the PsyPAH SBG is observed when compared to APF1 (Figure 6) arising from (i) displacement of P176-$V190^{PsyPAH}$ helix towards the catalytic domain (originating from the "closure" of the frontside of the E1 site by L179-$D208^{PsyPAH}$) and (ii) the presence of longer or more voluminous side chains at the backside of the E1 site (Figure 6).

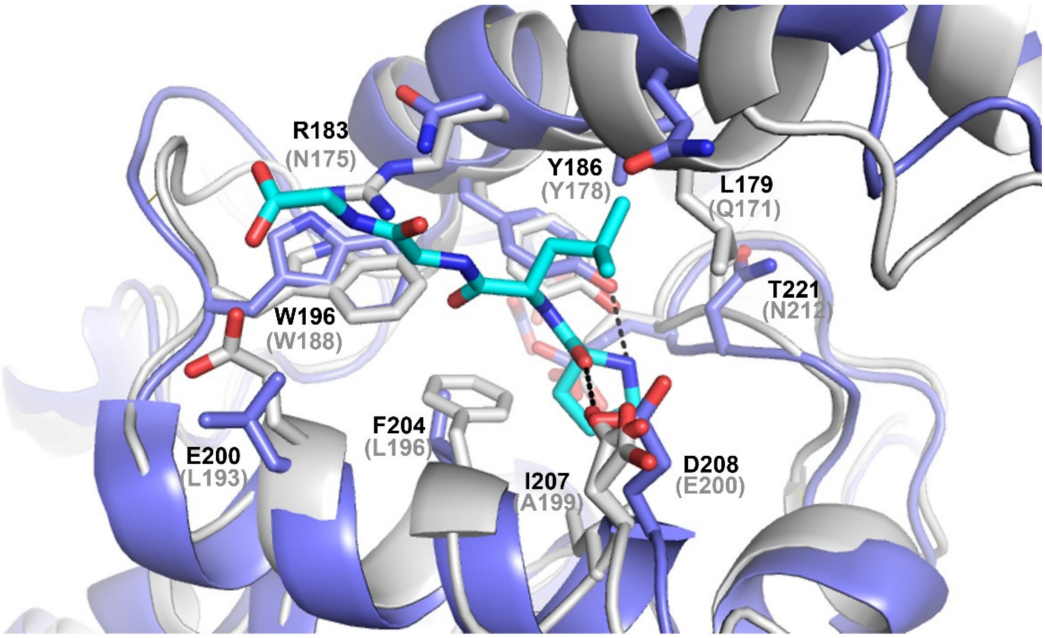

Figure 6. Superposition PsyPAH (white tones) and APF1 bound to PLGG peptide (PDB 1XQY, main chain in blue tones, peptide in sky blue tones). The numbering of the enzymes is that which appears in the corresponding PDBs (PsyPAH, black numbering; APF1, grey numbering).

R183^{PsyPAH} generates a stacking interaction with W196^{PsyPAH} (W188^{APF1}), closing the backside of the SBG, impeding the allocation of longer peptides. Residues L179^{PsyPAH} (Q171^{APF1}) and R183^{PsyPAH} (N175^{APF1}) would also hamper the presence of similar peptide ligands in PsyPAH (Figure 6). Finally, F204^{PsyPAH} (L196^{APF1}) and I207^{PsyPAH} (A199^{APF1}) reduce the SBG cleft volume, producing a higher hydrophobic character of this site compared to APF1, but lower than that presented by VinJ [18]. In fact, the hydrophobicity of this site would partly explain why PsyPAH can hydrolyze different aliphatic/aromatic amino acid amides, or even why the *p*-nitroanilide derivatives were hydrolyzed more efficiently than the amide derivatives (Table 2); the environment generated by Y186^{PsyPAH}, W196^{PsyPAH}, and F204^{PsyPAH} seems highly appropriate for the accommodation of an aromatic moiety. In this sense, it might be interesting to ascertain whereas other L-amino acid-amide derivatives with more voluminous amide substituents could be a more suitable starting material for their kinetic resolution using this subfamily of L-amidases. These differences in the SBG would support the different substrate specificity of PAHs when compared to PAPs.

3.5. Putative Catalytic Centre of PsyPAH

S113^{PsyPAH}, D253^{PsyPAH}, and H280^{PsyPAH} comprise the canonical clan SC class catalytic triad of the family (Table S3). The putative catalytic center of PsyPAH is buried into the structure, accessible through the deep hollow contiguous to the E1 site, where the substrate needs to enter to be cleaved. Whereas we were not able to obtain a ligand-bound structure through soaking experiments, an extra density was found at the S1 site in our crystallographic data, assigned as a phosphate molecule most likely arising from the initial purification buffer. This molecule is at a binding distance of N218^{PsyPAH} and E222^{PsyPAH} (Figures 7A and S5). Superposition with the APF1 bound to L-Proline reveals that both ligands occupy the same spatial position (Figure 7B). The counterpart of N209^{APF1} and E213^{APF1} residues were proved to be key for L-Pro-binding [55] together with Y205^{APF1} and E245^{APF1}. Since both enzymes process Pro-containing substrates and the four residues are conserved (N218^{PsyPAH}, E222^{PsyPAH}, Y214^{PsyPAH}, and E254^{PsyPAH}), a common L-Pro binding mode can be defined (Figure 7B).

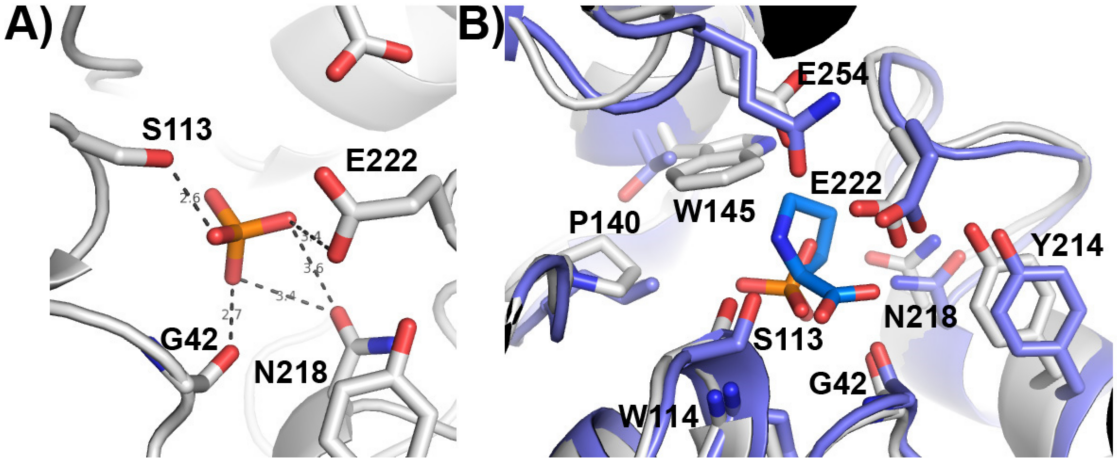

Figure 7. (**A**) Catalytic cleft of PsyPAH showing the modeled phosphate molecule. (**B**) Superposition of APF1 bound to L-Proline at the S1 site (PDB 1XRR, blue tones) and PsyPAH bound to phosphate (white tones). The numbering corresponds to PsyPAH residues.

Analogously to APF1, our structural model also supports the carbonyl/amide groups from the peptide bonds of G42^{PsyPAH} (G37^{APF1}) and W114^{PsyPAH} (Y106^{APF1}) as the constituents of the oxyanion hole (Figure 7A,B, Table S3). Despite the conservation of these key residues, the rest of the amino acids comprising S1 and S1′ sites are quite different (Table S3), while providing an overall hydrophobic character to these environments. It is important to highlight that P139^{PsyPAH} (L131^{APF1}) and W145^{PsyPAH} (T137^{APF1}) transform the PsyPAH S1 site into a much smaller and more hydrophobic cleft when compared to APF1, which might account for the substrate scope of PsyPAH toward different non-polar amides (see above).

Finally, further comparison of PsyPAH with SmPAP and XcPAP reveals that whereas the catalytic triad (S113^{PsyPAH}, D253^{PsyPAH}, and H280^{PsyPAH}) is positionally conserved in the catalytic domain, key binding residues of the cap domain (N218^{PsyPAH}, E222^{PsyPAH}, Y214^{PsyPAH}, and E254^{PsyPAH}, also present in APF1, VinJ, and MysPAP, Table S3), are not conserved. These results confirm the discussion about the PAP classification and provide additional clues on the different substrate scope observed among PAPs [56].

4. Conclusions

In conclusion, we report the first crystal structure of a PAP-like amidase (S33 peptidase clan) at 1.95 Å resolution with potential application within the "Amidase Process", showing a broad substrate specificity toward different canonical and non-canonical amino acids. Structural and sequence analyses allow one to decipher different L-amidase subfamilies, a prerequisite to finding enzymes with new or improved properties. Besides, the overall structure of PsyPAH is more similar to VinJ (a S33 peptidase, not a PAP), and structural comparison showed a higher conservation of key residues of the activity of APF1 (a S33 peptidase, not a strict PAP), suggesting a similar catalytic mechanism to that proposed for the latter. The lower volume and hydrophobicity of the S1 and E1 sites seem to account for the activity with smaller L-amino acid amides.

Therefore, our results confirm PsyPAH as a different member of the S33 peptidase family, which is not strictly a PAP enzyme. Future work should focus on understanding the substrate specificity of amidases conforming the S33 peptidase clan through mutational and structural studies. Since the divergence of the cap domain among these enzymes seems critical for substrate specificity, special attention should be taken to accurately classify them.

Supplementary Materials: The following are available online at https://www.mdpi.com/article/10.3390/cryst12010018/s1. Synthesis of different amino-acid amides. Figure S1: Kinetic determinations for L-Pro- and L-Leu-amide. Figure S2: Phylogenetic analysis of different enzymes with proven L-amidase activity. Figure S3: Surface representation of different peptidase S33 family members. Figure S4: Comparison of the polyketide substrate binding site of VinJ with that of APF1, MysPAP, and PsyPAH. Figure S5: Omit maps calculated for the PsyPAH structure. Table S1: Homolog structures of PsyPAH obtained with the DALI server. Table S2: Different ligand-bound structures of Tricorn Interacting Factor F1. Table S3: Residues involved in substrate binding and catalysis in the different pockets of APF1. Table S4: Comparison of residues proposed in the polyketide binding tunnel in VinJ.

Author Contributions: Conceptualization, S.M.-R. and J.A.G.; methodology, all authors; investigation, all authors; writing—original draft preparation, S.M.-R. and J.A.G.; writing—review and editing, all authors; funding acquisition, S.M.-R., R.C.-M., L.Á.d.C. and J.A.G. All authors have read and agreed to the published version of the manuscript.

Funding: This research was supported by the Spanish Ministry of Science and Innovation/FEDER funds grant PID2020-116261GB-I00/AEI/10.13039/501100011033 (JAG), from the FEDER/Junta de Andalucía-Consejería de Transformación Económica, Industria, Conocimiento y Universidades grants P18-FR-3533 (LAC) and P12-FQM-790 (RCM), and from the University of Granada grant PPJI2017-1 (SMR).

Institutional Review Board Statement: Not applicable.

Informed Consent Statement: Not applicable.

Data Availability Statement: Coordinates and structure factors have been deposited at the PDB with accession code 7A6G.

Acknowledgments: We are grateful to the European Synchrotron Radiation Facility (ESRF), Grenoble, France, for the provision of time through proposals Mx1938 and Mx2064, and the staff at ID30B beamline for their assistance during data collection. SMR and JTP are also grateful to the Andalusian Regional Government through the Endocrinology and Metabolism Group (CTS-202). We want to thank "Unidad de Excelencia Química aplicada a Biomedicina y Medioambiente" of the University of Granada.

Conflicts of Interest: The authors declare no conflict of interest. The funders had no role in the design of the study; in the collection, analyses, or interpretation of data; in the writing of the manuscript, or in the decision to publish the results.

References

1. Komeda, H.; Harada, H.; Washika, S.; Sakamoto, T.; Ueda, M.; Asano, Y. S-stereoselective piperazine-2-tert-butylcarboxamide hydrolase from *Pseudomonas azotoformans* IAM 1603 is a novel L-amino acid amidase. *Eur. J. Biochem.* **2004**, *271*, 1465–1475. [CrossRef] [PubMed]
2. Komeda, H.; Hariyama, N.; Asano, Y. L-Stereoselective amino acid amidase with broad substrate specificity from *Brevundimonas diminuta*: Characterization of a new member of the leucine aminopeptidase family. *Appl. Microbiol. Biotechnol.* **2006**, *70*, 412–421. [CrossRef] [PubMed]
3. Yamaguchi, S.; Komeda, H.; Asano, Y. New enzymatic method of chiral amino acid synthesis by dynamic kinetic resolution of amino acid amides: Use of stereoselective amino acid amidases in the presence of alpha-amino-epsilon-caprolactam racemase. *Appl. Environ. Microbiol.* **2007**, *73*, 5370–5373. [CrossRef] [PubMed]
4. Martínez-Rodríguez, S.; Torres, J.M.; Sánchez, P.; Ortega, E. Overview on Multienzymatic Cascades for the Production of Non-canonical α-Amino Acids. *Front. Bioeng. Biotechnol.* **2020**, *8*, 887. [CrossRef]
5. Hamer, D.; Greenstein, J.P. An enzymatic resolution of proline. *J. Biol. Chem.* **1951**, *193*, 81–89. [CrossRef]
6. Work, E.; Birnbaum, S.; Winitz, M.; Greenstein, J. Separation of the Three Isomeric Components of Synthetic α, ε-Diaminopimelic Acid1. *J. Am. Chem. Soc.* **1955**, *77*, 1916–1918. [CrossRef]
7. Sonke, T.; Ernste, S.; Tandler, R.F.; Kaptein, B.; Peeters, W.P.; van Assema, F.B.; Wubbolts, M.G.; Schoemaker, H.E. L-selective amidase with extremely broad substrate specificity from *Ochrobactrum anthropi* NCIMB 40321. *Appl. Environ. Microbiol.* **2005**, *71*, 7961–7973. [CrossRef] [PubMed]
8. van den Tweel, W.J.J.; van Dooren, T.J.G.M.; de Jonge, P.H.; Kaptein, B.; Duchateau, A.L.L.; Kamphuis, K. *Ochrobactrum anthropi* NCIMB 40321: A new biocatalyst with broad-spectrum l-specific amidase activity. *Appl. Microbiol. Biotechnol.* **1993**, *39*, 296–300. [CrossRef]

9. Hermes, H.F.; Sonke, T.; Peters, P.J.; van Balken, J.A.; Kamphuis, J.; Dijkhuizen, L.; Meijer, E.M. Purification and Characterization of an l-Aminopeptidase from *Pseudomonas putida* ATCC 12633. *Appl. Environ. Microbiol.* **1993**, *59*, 4330–4334. [CrossRef] [PubMed]
10. Hermes, H.F.; Tandler, R.F.; Sonke, T.; Dijkhuizen, L.; Meijer, E.M. Purification and Characterization of an l-Amino Amidase from *Mycobacterium neoaurum* ATCC 25795. *Appl. Environ. Microbiol.* **1994**, *60*, 153–159. [CrossRef]
11. Kamphuis, J.; Meijer, E.M.; Boesten, W.H.J.; Broxterman, Q.B.; Kaptein, B.; Hermes, H.F.M.; Schoemaker, H.E. Production of natural and synthetic L- and D-amino acids by aminopeptidases and amino amidases. In *Biocatalytic Production of Amino Acids and Derivatives*; Rozzell, J.D., Wagner, F., Eds.; Wiley: New York, NY, USA, 1992; pp. 178–206.
12. Maestracci, M.; Bui, K.; Thiéry, A.; Arnaud, A.; Galzy, P. The amidases from a *Brevibacterium strain*: Study and applications. *Adv. Biochem. Eng. Biotechnol.* **1988**, *36*, 67–115. [CrossRef] [PubMed]
13. Youshko, M.I.; Luuk, M.; Sheldon, R.A.; Švedas, V.K. Application of aminoacylase I to the enantioselective resolution of α-amino acid esters and amides. *Tetrahedron Asymmetry* **2004**, *15*, 1933–1936. [CrossRef]
14. Stelkes-Ritter, U.; Beckers, G.; Bommarius, A.; Drauz, K.; Günther, K.; Kottenhahn, M.; Schwarm, M.; Kula, M.R. Kinetics of Peptide Amidase and its Application for the Resolution of Racemates. *Biocatal. Biotransform.* **2009**, *15*, 205–219. [CrossRef]
15. Mahon, C.S.; O'Donoghue, A.J.; Goetz, D.H.; Murray, P.G.; Craik, C.S.; Tuohy, M.G. Characterization of a multimeric, eukaryotic prolyl aminopeptidase: An inducible and highly specific intracellular peptidase from the non-pathogenic fungus *Talaromyces emersonii*. *Microbiology* **2009**, *155*, 3673–3682. [CrossRef] [PubMed]
16. Inoue, T.; Ito, K.; Tozaka, T.; Hatakeyama, S.; Tanaka, N.; Nakamura, K.T.; Yoshimoto, T. Novel inhibitor for prolyl aminopeptidase from *Serratia marcescens* and studies on the mechanism of substrate recognition of the enzyme using the inhibitor. *Arch. Biochem. Biophys.* **2003**, *416*, 147–154. [CrossRef]
17. Tamura, T.; Tamura, N.; Lottspeich, F.; Baumeister, W. Tricorn protease (TRI) interacting factor 1 from *Thermoplasma acidophilum* is a proline iminopeptidase. *FEBS Lett.* **1996**, *398*, 101–105. [CrossRef]
18. Shinohara, Y.; Miyanaga, A.; Kudo, F.; Eguchi, T. The crystal structure of the amidohydrolase VinJ shows a unique hydrophobic tunnel for its interaction with polyketide substrates. *FEBS Lett.* **2014**, *588*, 995–1000. [CrossRef] [PubMed]
19. Ezawa, T.; Jung, S.; Kawashima, Y.; Noguchi, T.; Imai, N. Convenient green preparation of dipeptides using unprotected α-amino acids. *Tetrahedron Asymmetry* **2017**, *28*, 75–83. [CrossRef]
20. Riley, J.P. The spectrophotometric determination of ammonia in natural waters with particular reference to sea-water. *Anal. Chim. Acta* **1953**, *9*, 575–589. [CrossRef]
21. Erlanger, B.F.; Kokowsky, N.; Cohen, W. The preparation and properties of two new chromogenic substrates of trypsin. *Arch. Biochem. Biophys.* **1961**, *95*, 271–278. [CrossRef]
22. Kabsch, W. XDS. *Acta Cryst. D Biol. Cryst.* **2010**, *66*, 125–132. [CrossRef]
23. Winn, M.D.; Ballard, C.C.; Cowtan, K.D.; Dodson, E.J.; Emsley, P.; Evans, P.R.; Keegan, R.M.; Krissinel, E.B.; Leslie, A.G.; McCoy, A.; et al. Overview of the CCP4 suite and current developments. *Acta Cryst. D Biol. Cryst.* **2011**, *67*, 235–242. [CrossRef] [PubMed]
24. Bunkóczi, G.; Echols, N.; McCoy, A.J.; Oeffner, R.D.; Adams, P.D.; Read, R.J. Phaser.MRage: Automated molecular replacement. *Acta Cryst. D Biol. Cryst.* **2013**, *69*, 2276–2286. [CrossRef] [PubMed]
25. Afonine, P.V.; Grosse-Kunstleve, R.W.; Echols, N.; Headd, J.J.; Moriarty, N.W.; Mustyakimov, M.; Terwilliger, T.C.; Urzhumtsev, A.; Zwart, P.H.; Adams, P.D. Towards automated crystallographic structure refinement with phenix.refine. *Acta Cryst. D Biol. Cryst.* **2012**, *68*, 352–367. [CrossRef] [PubMed]
26. Murshudov, G.N.; Skubák, P.; Lebedev, A.A.; Pannu, N.S.; Steiner, R.A.; Nicholls, R.A.; Winn, M.D.; Long, F.; Vagin, A.A. REFMAC5 for the refinement of macromolecular crystal structures. *Acta Cryst. D Biol. Cryst.* **2011**, *67*, 355–367. [CrossRef]
27. Emsley, P.; Lohkamp, B.; Scott, W.G.; Cowtan, K. Features and development of Coot. *Acta Cryst. D Biol. Cryst.* **2010**, *66*, 486–501. [CrossRef] [PubMed]
28. Painter, J.; Merritt, E.A. Optimal description of a protein structure in terms of multiple groups undergoing TLS motion. *Acta Cryst. D Biol. Cryst.* **2006**, *62*, 439–450. [CrossRef]
29. Chen, V.B.; Arendall, W.B.; Headd, J.J.; Keedy, D.A.; Immormino, R.M.; Kapral, G.J.; Murray, L.W.; Richardson, J.S.; Richardson, D.C. MolProbity: All-atom structure validation for macromolecular crystallography. *Acta Cryst. D Biol. Cryst.* **2010**, *66*, 12–21. [CrossRef]
30. Laskowski, R.A.; Jabłońska, J.; Pravda, L.; Vařeková, R.S.; Thornton, J.M. PDBsum: Structural summaries of PDB entries. *Protein Sci.* **2018**, *27*, 129–134. [CrossRef]
31. Madeira, F.; Park, Y.M.; Lee, J.; Buso, N.; Gur, T.; Madhusoodanan, N.; Basutkar, P.; Tivey, A.R.N.; Potter, S.C.; Finn, R.D.; et al. The EMBL-EBI search and sequence analysis tools APIs in 2019. *Nucleic Acids Res.* **2019**, *47*, W636–W641. [CrossRef]
32. Robert, X.; Gouet, P. Deciphering key features in protein structures with the new ENDscript server. *Nucleic Acids Res.* **2014**, *42*, W320–W324. [CrossRef] [PubMed]
33. Letunic, I.; Bork, P. Interactive Tree Of Life (iTOL) v4: Recent updates and new developments. *Nucleic Acids Res.* **2019**, *47*, W256–W259. [CrossRef] [PubMed]
34. Holm, L. DALI and the persistence of protein shape. *Protein Sci.* **2020**, *29*, 128–140. [CrossRef] [PubMed]
35. The Pymol Molecular Graphics System, Schrödinger, LLC. Available online: https://www.scirp.org/(S(vtj3fa45qm1ean45vvffcz55))/reference/ReferencesPapers.aspx?ReferenceID=1958992 (accessed on 25 November 2021).
36. Stetefeld, J.; McKenna, S.A.; Patel, T.R. Dynamic light scattering: A practical guide and applications in biomedical sciences. *Biophys. Rev.* **2016**, *8*, 409–427. [CrossRef]

37. Wu, Z.; Liu, C.; Zhang, Z.; Zheng, R.; Zheng, Y. Amidase as a versatile tool in amide-bond cleavage: From molecular features to biotechnological applications. *Biotechnol. Adv.* **2020**, *43*, 107574. [CrossRef]
38. Wagner, F.W.; Wilkes, S.H.; Prescott, J.M. Specificity of *Aeromonas* aminopeptidase toward amino acid amides and dipeptides. *J. Biol. Chem.* **1972**, *247*, 1208–1210. [CrossRef]
39. Nandan, A.; Nampoothiri, K.M. Molecular advances in microbial aminopeptidases. *Bioresour. Technol.* **2017**, *245*, 1757–1765. [CrossRef]
40. Nandan, A.; Nampoothiri, K.M. Therapeutic and biotechnological applications of substrate specific microbial aminopeptidases. *Appl. Microbiol. Biotechnol.* **2020**, *104*, 5243–5257. [CrossRef]
41. Inoue, A.; Komeda, H.; Asano, Y. Asymmetric Synthesis of L-α-Methylcysteine with the Amidase from *Xanthobacter flavus* NR303. *Adv. Synth. Catal.* **2005**, *347*, 1132–1138. [CrossRef]
42. Matsushima, M.; Takahashi, T.; Ichinose, M.; Miki, K.; Kurokawa, K.; Takahashi, K. Structural and immunological evidence for the identity of prolyl aminopeptidase with leucyl aminopeptidase. *Biochem. Biophys. Res. Commun.* **1991**, *178*, 1459–1464. [CrossRef]
43. Nakamura, T.; Yu, F. Amidase Gene. U.S. Patent 6617139, 9 September 2003.
44. Katoh, O.; Akiyama, T.; Nakamura, T. Novel Amide Hydrolase Gene. EP Patent Application EP1428876A1, 16 June 2004.
45. Asano, Y. L-Amino Acid Amide Asymmetric Hydrolase and Dna Encoding the Same. EP1770166A4, 19 December 2007.
46. Matsushima, M.; Takahashi, T.; Ichinose, M.; Miki, K.; Kurokawa, K.; Takahashi, K. Prolyl aminopeptidases from pig intestinal mucosa and human liver: Purification, characterization and possible identity with leucyl aminopeptidase. *Biomed. Res.* **1991**, *12*, 323–333. [CrossRef]
47. Rawlings, N.D.; Barrett, A.J.; Thomas, P.D.; Huang, X.; Bateman, A.; Finn, R.D. The MEROPS database of proteolytic enzymes, their substrates and inhibitors in 2017 and a comparison with peptidases in the PANTHER database. *Nucleic Acids Res.* **2018**, *46*, D624–D632. [CrossRef]
48. Holmquist, M. Alpha/Beta-hydrolase fold enzymes: Structures, functions and mechanisms. *Curr. Protein Pept. Sci.* **2000**, *1*, 209–235. [CrossRef] [PubMed]
49. Marchot, P.; Chatonnet, A. Enzymatic activity and protein interactions in alpha/beta hydrolase fold proteins: Moonlighting versus promiscuity. *Protein Pept. Lett.* **2012**, *19*, 132–143. [CrossRef] [PubMed]
50. Goettig, P.; Groll, M.; Kim, J.S.; Huber, R.; Brandstetter, H. Structures of the tricorn-interacting aminopeptidase F1 with different ligands explain its catalytic mechanism. *EMBO J.* **2002**, *21*, 5343–5352. [CrossRef]
51. Lenfant, N.; Hotelier, T.; Velluet, E.; Bourne, Y.; Marchot, P.; Chatonnet, A. ESTHER, the database of the α/β-hydrolase fold superfamily of proteins: Tools to explore diversity of functions. *Nucleic Acids Res.* **2013**, *41*, D423–D429. [CrossRef]
52. Medrano, F.J.; Alonso, J.; García, J.L.; Romero, A.; Bode, W.; Gomis-Rüth, F.X. Structure of proline iminopeptidase from *Xanthomonas campestris* pv. citri: A prototype for the prolyl oligopeptidase family. *EMBO J.* **1998**, *17*, 1–9. [CrossRef] [PubMed]
53. Yoshimoto, T.; Kabashima, T.; Uchikawa, K.; Inoue, T.; Tanaka, N.; Nakamura, K.T.; Tsuru, M.; Ito, K. Crystal structure of prolyl aminopeptidase from *Serratia marcescens*. *J. Biochem.* **1999**, *126*, 559–565. [CrossRef]
54. Okai, M.; Miyauchi, Y.; Ebihara, A.; Lee, W.C.; Nagata, K.; Tanokura, M. Crystal structure of the proline iminopeptidase-related protein TTHA1809 from *Thermus thermophilus* HB8. *Proteins* **2008**, *70*, 1646–1649. [CrossRef] [PubMed]
55. Goettig, P.; Brandstetter, H.; Groll, M.; Göhring, W.; Konarev, P.V.; Svergun, D.I.; Huber, R.; Kim, J.S. X-ray snapshots of peptide processing in mutants of tricorn-interacting factor F1 from *Thermoplasma acidophilum*. *J. Biol. Chem.* **2005**, *280*, 33387–33396. [CrossRef]
56. Ito, K.; Inoue, T.; Kabashima, T.; Kanada, N.; Huang, H.S.; Ma, X.; Azmi, N.; Azab, E.; Yoshimoto, T. Substrate recognition mechanism of prolyl aminopeptidase from *Serratia marcescens*. *J. Biochem.* **2000**, *128*, 673–678. [CrossRef] [PubMed]